ELSEVIER

Materials Science and Engineering A293 (2000) 267–274

MATERIALS SCIENCE & ENGINEERING A

www.elsevier.com/locate/msea

Characterization and modeling of precipitation kinetics in an Al–Zn–Mg alloy

J.C. Werenskiold, A. Deschamps *, Y. Bréchet

LTPCM/ENSEEG, UMR 5614, Domaine Universitaire, BP75, 38 402 St Martin d'Hères Cedex, France

Received 1 November 1999; received in revised form 17 April 2000

Abstract

The precipitation kinetics in AA7108.70 Al–Zn–Mg alloy have been investigated by small angle X-ray scattering and transmission electron microscopy, and computer modeled by use of an internal state variable model concerning two regimes, (i) precipitation and growth and (ii) growth and coarsening. The modeling and experiments were done for isothermal heat treatment at 120, 140, 150, 160 and 170°C. These treatments were also compared with the industrial two step T6 treatment.

Keywords: Al–Zn–Mg alloy; Precipitation kinetics; Isothermal heat treatments; Modeling; Small angle scattering

1. Introduction

Al–Zn–Mg alloys are used for structural applications in the aerospace and automotive industry. They present a wide range of potential applications due to their high specific mechanical properties. The present study is related to alloys used in car bumpers. The process route of these materials involves a solution treatment followed by a rapid quench, a forming operation involving some plastic strain, and finally a precipitation treatment to increase the strength of the bumper to the required level. This heat treatment is performed over a wide range of temperatures, usually in several steps. The first step ranges from 100 to 120°C which is within the stability range of GP-zones [1], and the second step from 140 to 170°C which is the temperature range for η' and η precipitation [2].

In order to optimize and control the thermal sequence of the heat treatment, it is necessary to understand which phases are present at the different steps of the heat treatment, and the kinetics of precipitation at the different temperatures involved. The first necessary step to reach this goal is to measure in a quantitative manner how sensitive the precipitation reaction is to the important changes in nucleation conditions which are encountered at the different temperatures [3]. The second step is to describe these experimental results by a model capable of predicting the effect of nucleation on precipitation kinetics.

The purpose of present work is to investigate experimentally the isothermal precipitation behavior in the alloy AA7108.70 over the temperature range 120–170°C, and to apply on the quantitative data obtained the modeling approach, which has been developed previously [4] by two of the authors. The aim of the present modeling work is to investigate the temperature dependence of physical parameters such as nucleation barrier in order to get insight in the physical mechanisms involved.

2. Materials and methods

The 7108.70 alloy was provided by Hydro-Raufoss Automotive Research Center as extruded plates. Alloy composition is 5.5%Zn, 1.2%Mg, 0.16%Zr and 0.15%Fe (all in wt.%). The solution treatment was 30 min at 480°C followed by water quenching, and resulted in a fully fibrous structure, with an average subgrain size of approximately 3.5 μm.

* Corresponding author. Fax: +33-4-76826644.
E-mail address: alexis.deschamps@ltpcm,inpg.fr (A. Deschamps).

0921-5093/00/$ - see front matter
PII: S0921-5093(00)01247-8

Isothermal heat treatments were mainly studied. They consisted simply of 2 h at room temperature, followed by a fast heating ramp of 320°C h^{-1} up to the desired temperature (120, 140, 150, 160 and 170°C). The isothermal precipitation behavior was then compared with the industrial two step T6 heat treatment. The T6 treatment consists of 2 h natural aging, followed by 6 h at 100°C, 24 h at room temperature and 6 h at 150°C (inserted to hot furnace).

The nature and distribution of precipitates were investigated by transmission electron microscopy (TEM) after 7 h at 120, 150 and 170°C and in the T6 state. Samples were prepared by ultrasonic cutting of 3 mm discs and electropolishing in a double-jet Tenupol by a 33% nitric acid solution in methanol maintained at −20°C and 15 V. Samples were observed on a Jeol 3010 microscope.

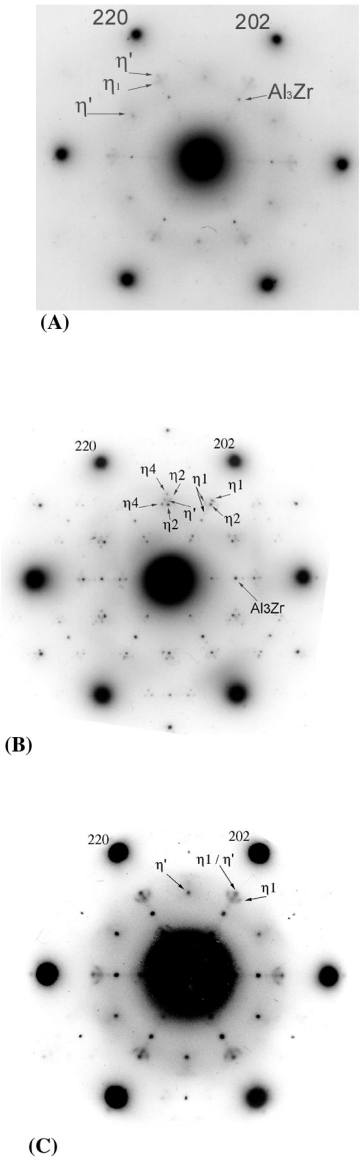

Fig. 1. (a) ⟨111⟩ Diffraction pattern from the 7 h at 150°C showing mostly η' and some η. (b) ⟨111⟩ Diffraction pattern from the 7 h at 170°C showing η spots in the orientations 1, 2 and 4. (c) Diffraction pattern from the T6 sample showing very clear η' spots.

The precipitation kinetics was investigated by small angle X-ray scattering (SAXS) performed in situ during the heat treatment. A conventional X-ray tube with Cu anode was used with Ni filters in order to get a Cu K_α source ($\lambda = 1.541$ Å). A position sensitive detector was used to measure the scattering vector q ranging from 0.02 to 0.5 $Å^{-1}$. Spectra were corrected for background, fluorescence and absorption effects.

The particle dimensions were calculated using the Guinier approximation, which gives the gyration radius of the particles [5].

$$I \propto \exp\left(-\frac{q^2R^2}{3}\right) \quad (1)$$

The Guinier plot ($\ln(I)$ vs. q^2) shows a straight line in a wide range of scattering vectors, typically in the range $0.8 < qR < 2$, where R is the effective precipitate radius $(\langle R^8\rangle/\langle R^6\rangle)^{1/2}$ and q the scattering vector. For spherical particles, the gyration radius is $\sqrt{(3/5)}$ of the effective radius, however, TEM observations showed that the precipitates can be approximated as ellipsoids with half axes 6:6:1. The gyration radius then becomes approximately equal to the radius of a sphere with equal volume, thus, in the following we will consider that the gyration radius and the precipitate equivalent radius are identical and use the same symbol R for both parameters. Finally, the integrated intensity $Q_0 = \int_0^\infty Iq^2\,dq$ was also calculated from the X-ray scattering spectra and related to the volume fraction through the following equation:

$$Q_0 = 2\pi^2 f_v(1-f_v)\frac{(\Delta Z)^2}{\Omega^2} \quad (2)$$

where f_v is the precipitated volume fraction, Ω the atomic volume ($= 16.5$ $Å^{-3}$) and ΔZ is the difference in average atomic number between the precipitates and matrix, which was calculated assuming that the precipitates had the composition of the equilibrium η phase $MgZn_2$.

3. Transmission electron microscopy

Transmission electron microscopy (TEM) was first carried out on samples in the as-quenched state. The material shows a typical extrusion structure with elongated sub-grains. As expected, numerous Al_3Zr dispersoids can be seen on grain and sub-grain boundaries showing a very effective pinning [6].

Diffraction on samples with 7 h at 120°C did not show any traces of η' precipitates. Some very diffuse spots are indicating some GP(II). In bright field, we can observe precipitates with size corresponding to the

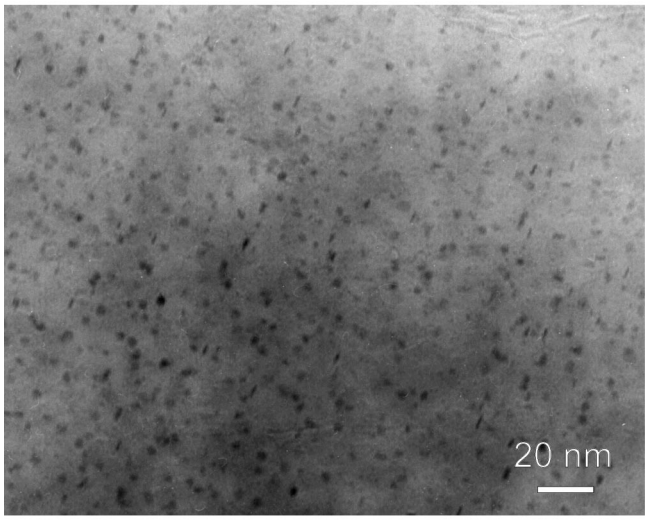

(A)

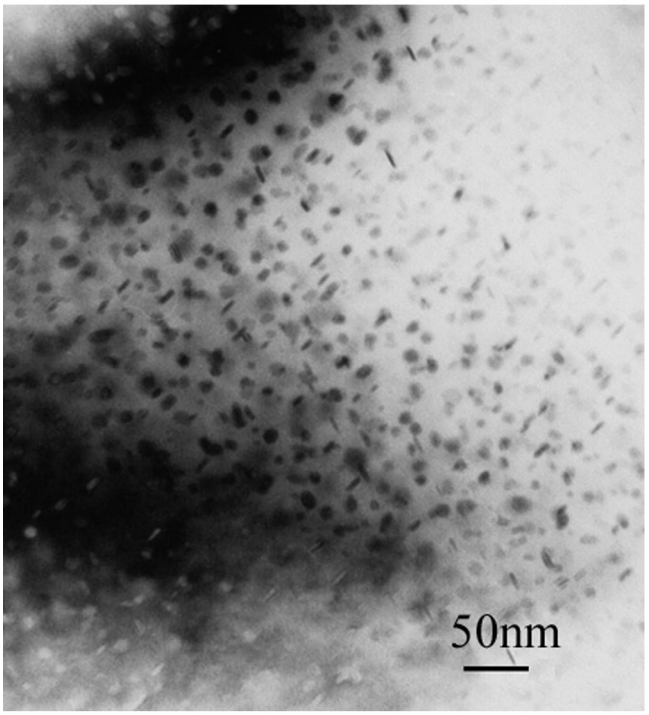

(B)

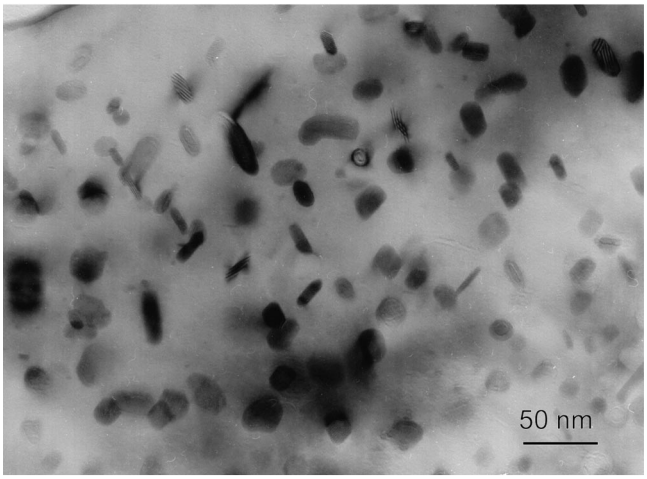

(C)

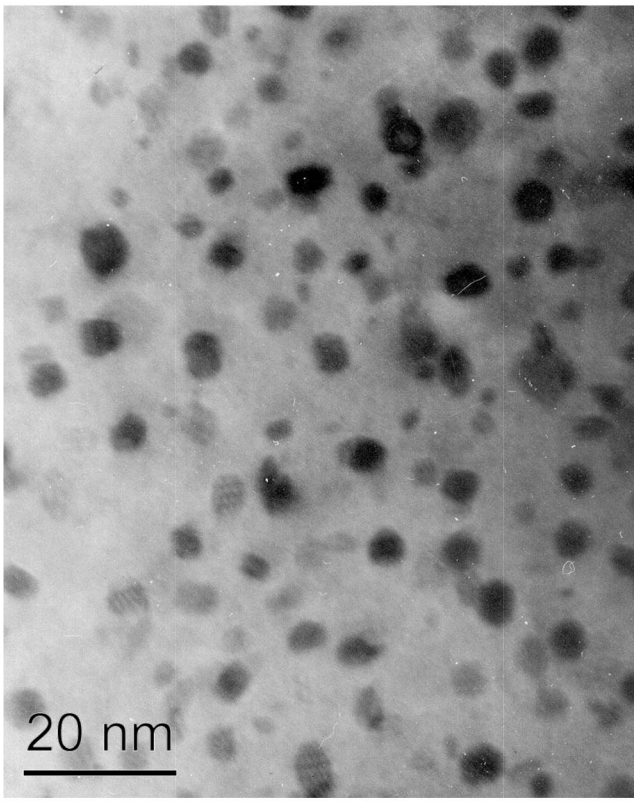

(D)

Fig. 2. (a) Bright field of GP zones in the 7 h at 120°C sample. (b) Bright field of precipitates in the 7 h at 150°C sample. (c) Bright field of precipitates in the 7 h at 170°C sample. (d) Bright field of the precipitates in the T6 sample.

SAXS results. This confirms another study [7] on the same alloy, which shows that the precipitates after 1 h at either 100 or 130°C consist of GP(I) and some GP(II) zones.

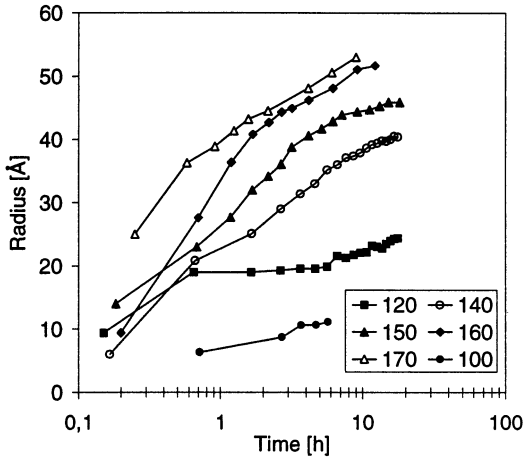

Fig. 3. Precipitate radius as function of aging time for all temperatures investigated from the SAXS experiments.

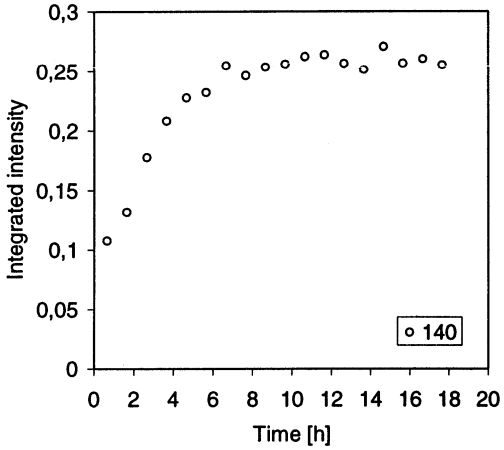

Fig. 4. Integrated intensity from the 140°C sample.

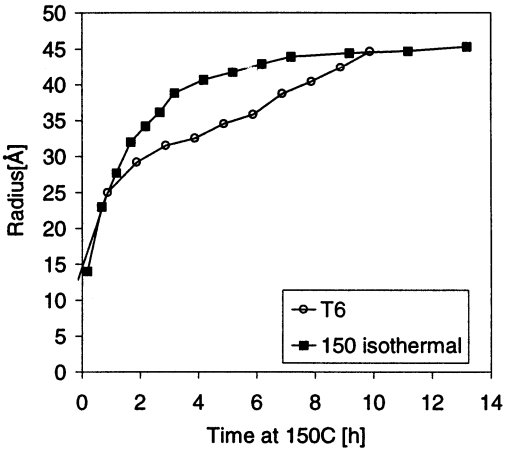

Fig. 5. Comparison between the 150°C isothermal and the second step of the T6 treatment showing a refining effect of the 100°C pre heat treatment in the case of T6.

After 7 h at 150°C the microstructure consisted of a uniform distribution of precipitates, except for a small precipitate-free zone of the order of 40 nm center to edge around the grain boundaries. The nature of precipitates was obtained from the $[111]_{Al}$ diffraction pattern [8,9](Fig. 1a). This pattern shows mostly the characteristic $\{2\bar{1}\bar{1}0\}_{\eta'}$ spots. A very small amount of η_1 precipitates can be detected as well, but in much smaller proportions as compared with η'.

The material aged 7 h at 170°C shows also a uniform dispersion of precipitates (Fig. 1b). The diffraction analysis in the $[111]_{Al}$ pattern presents a different situation as compared with the 150°C state. The precipitates appear to be η in the orientations η_1, η_2 and η_4.

Finally, the T6 material showed a very similar microstructure to the 150°C material, mostly η' and a small amount of η (Fig. 1c).

Bright field images from the four states are shown in Fig. 2a–d.

4. SAXS investigation

The evolution of the precipitate radius with isothermal aging time at the different temperatures is shown in Fig. 3. At 100 and 120°C the precipitate size does not show significant evolution from the nucleation radius during the heat treatment. At higher temperatures the precipitate radius increases rapidly from the nucleation radius.

We have represented in Fig. 4 the evolution of the integrated intensity for the 140°C heat treatment. It increases steadily with aging time and saturates after approximately 6 h at 140°C, suggesting that after 6 h the system enter a coarsening regime. A similar behavior can be observed at all temperatures higher than 120°C.

In situ measurements were also performed on the T6 heat treatment. The result in terms of precipitate radius is shown in Fig. 5, along with the isothermal 150°C treatment. For an identical time at 150°C, the T6 treatment results systematically in a smaller precipitate radius, indicating that there is a persistent refining effect of the first precipitation treatment at 100°C in the T6 heat treatment.

5. Discussion and modeling of precipitation kinetics

Before proceeding with modeling of the precipitation kinetics as obtained by SAXS results, it is useful to discuss the precipitation sequence at the different temperatures involved. There are two alternative routes for η' formation [10] as illustrated in Fig. 6.

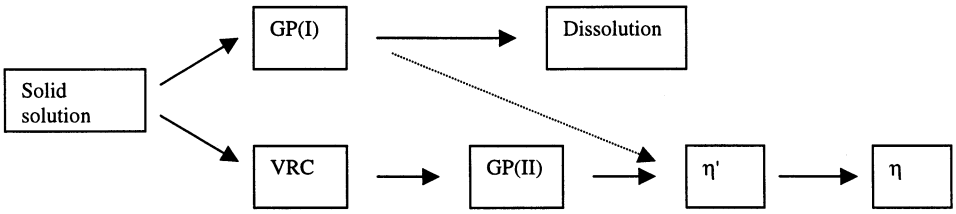

Fig. 6. Precipitation sequence in the Al–Zn–Mg alloys.

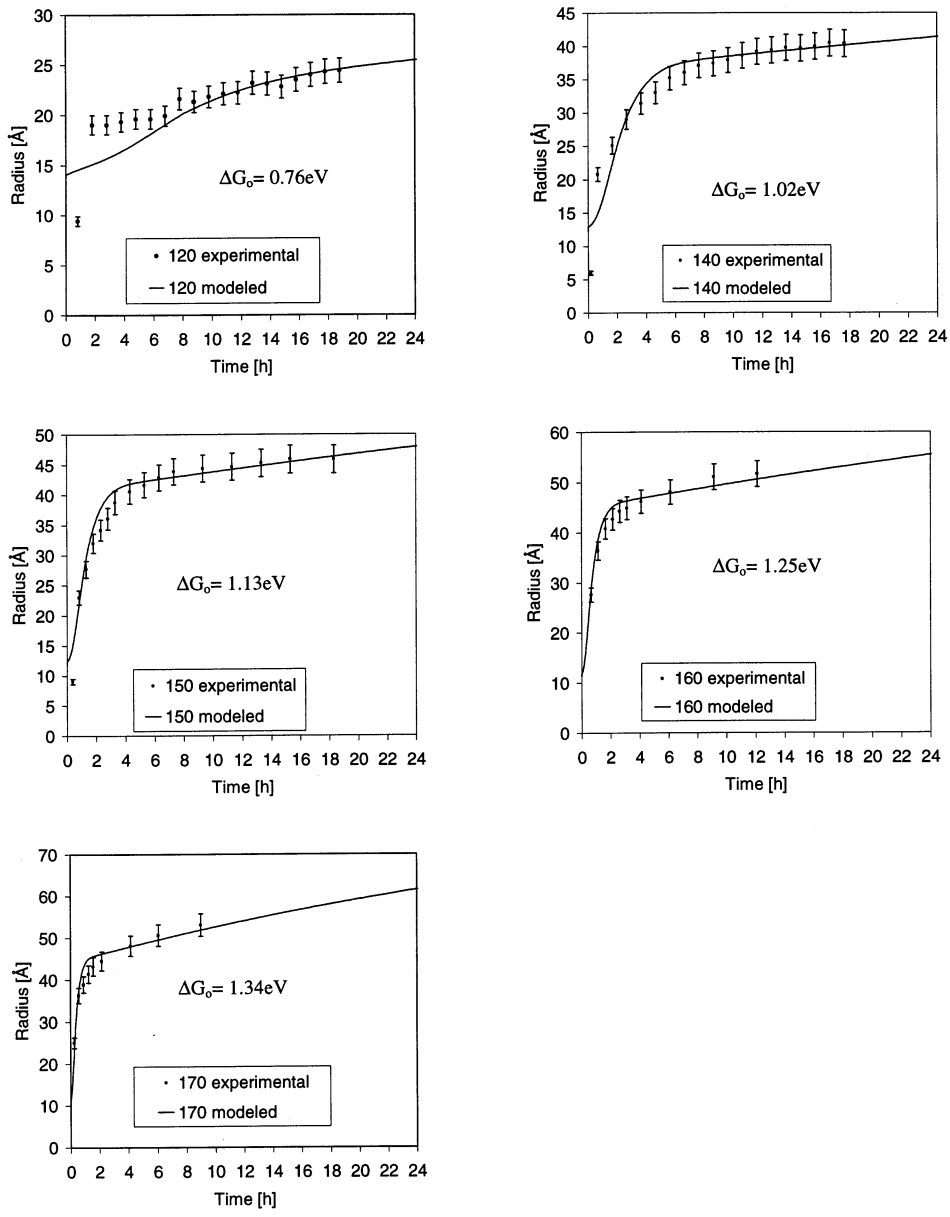

Fig. 7. (a–e) Results of the modeling, experimental results of the precipitate radius along with the best fit from the model.

After solution treatment followed by quenching to RT, there will be a supersaturation of vacancies and alloying elements in the alloy. Two types of zones or clusters are formed at RT — GP(I)-zones and 'vacancy rich clusters' called VRC. The VRC are thought to be formed right after or during the quench to RT and to be quite stable at this temperature. They are assumed to constitute the main formation route to η' with GP(II) zones as an intermediate phase. At higher aging temperatures, above the GP zone solvus, GP(II) transforms into η' while GP(I) either dissolves or transform into η' if it has reached some critical size [11].

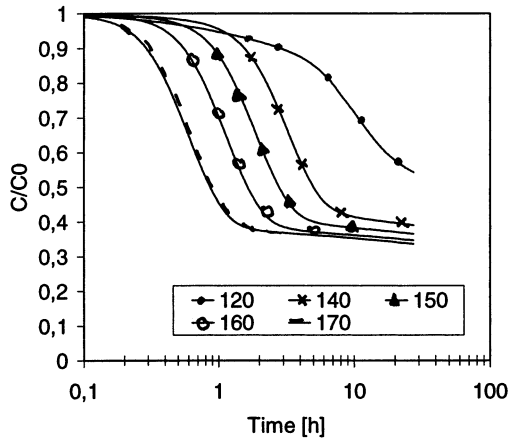

Fig. 8. Evolution of the solute decay as a function of aging time and temperature as suggested by the model.

The η' precipitates can appear as the nucleated phase at up to 180°C. During the course of the isothermal heat treatment, they are replaced by the equilibrium η phase. It is not clear what the lower limit in temperature is for this transformation, however, this transformation does not seem to be of great importance for practical purposes, it has never been shown that it changed either the precipitation kinetics (through a change in coherency strains and interfacial energy), either the hardening potential of the alloy. In contrast the GP $\rightarrow \eta'$ transition is of great importance both for the kinetics of precipitation and for the hardening behavior.

We have seen that the material in the T6 condition (i.e. after 6 h at 100°C and 6 h at 150°C) and the isothermal 7 h at 150°C consisted mostly of η' precipitates, which indeed are considered to offer the maximum hardening potential [12]. After 7 h at 170°C, most of the precipitates are η_1, which are probably the result of a transformation of earlier η' precipitates.

For the isothermal heat treatments, we summarize as follows the information provided by our investigation, at 100°C the precipitates are most certainly GP zones [1]. At 120°C precipitation starts with GP zones and even if it is likely that these GP zones undergo transformation into η' precipitates after longer aging time, no traces of η' could be seen in diffraction after 6 h at 120°C. At higher temperatures the system is above the GP zone solvus. It is likely that nucleation of η' will occur on clusters/zones which have formed during either the 2 h of natural aging or during the quench [13].

5.1. Modeling approach

The analysis of the SAXS data will be done using a model that has been developed for another 7000 series aluminum alloy, which contained higher levels of solute. This modeling approach was applied to isothermal heat treatments at a single temperature, 160°C. One aim of the present modeling work is to know the flexibility of the precipitation model, especially in terms of changing the heat treatment temperature which will influence many parameters, such as diffusion, equilibrium concentration in solute, and nucleation mechanisms.

Let us first recall the main assumptions of the model [4]. The first important simplification is that the ternary nature of the alloy is not taken into account, the alloy is considered to be pseudo-binary, with an equivalent solute having its own equilibrium concentration and diffusion constant. In this framework, the precipitates are supposed to be pure solute. The second simplification is that the complex sequence of precipitation is replaced by a single precipitation process (which is supposed to be η'). The GP zones (or if they are absent, the VRCs) are not considered directly, but enter the model as nucleation sites for the η' precipitates. The transition of η' into η is not considered.

In the following equations describing the model, T is the absolute temperature, k Boltzmann's constant, v_{at} the average atomic volume (supposed identical in the precipitate and the matrix), C the solute concentration in the matrix at time t, C_{eq} the equilibrium solute

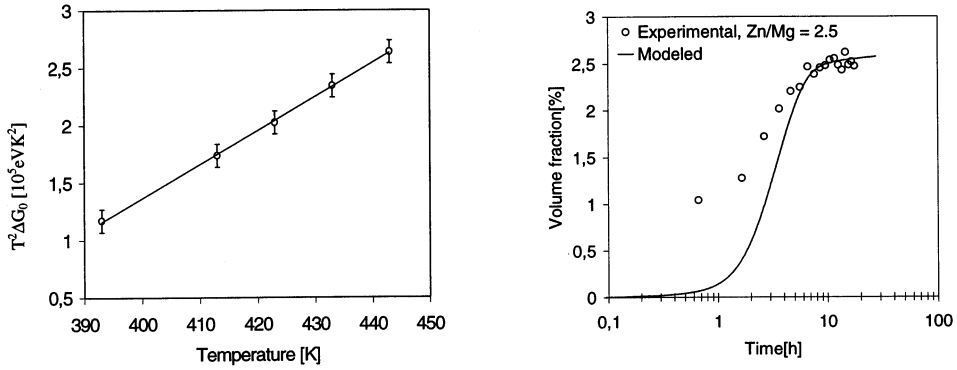

Fig. 9. (a) A plot of $T^2\Delta G^0$ vs. T, showing a straight line, indicating that the nucleation is more difficult at higher temperatures. (b) Callculated precipitated volume fraction from the model and from the integrated intensity for the 140°C heat treatment.

concentration, C_0 the initial concentration, γ the interfacial energy between precipitate and matrix, Z the Zeldovich factor, N_0 the number of atoms by unit volume, N the precipitate density, R^* the critical radius for both nucleation and coarsening, and finally, ΔG_0 is an adjustable parameter reflecting the heterogeneous nature of the nucleation mechanism, and is expected to depend on the nucleation conditions.

Following these thermodynamic considerations, the model includes two steps, a step combining nucleation and growth of precipitates, followed by a step combining growth and coarsening. The details of the model can be found in [4].

The activation energy for nucleation from an ideal solution model is given by.

$$\Delta G^* = \frac{\Delta G_0}{\ln^2(C/C_{eq})} \tag{3}$$

In the nucleation and growth regime the following equations are used. For the nucleation rate, a standard Becker–Döring law is taken:

$$\left.\frac{dN}{dt}\right|_{nucleation} = N_0 Z \beta^* \exp\left(-\frac{\Delta G^*}{kT}\right)\exp\left(-\frac{\tau}{t}\right)$$

$$\beta^* = \frac{4\pi R^{*2} D C_0}{a^4}$$

$$\tau = \frac{1}{2\beta^* Z} \tag{4}$$

The evolution of precipitate radius is given as

$$\frac{dR}{dt} = \frac{D}{R}\frac{C - C_{eq}\exp(R_0/R)}{1 - C_{eq}\exp(R_0/R)} + \frac{1}{N}\frac{dN}{dt}\left(\alpha\frac{R_0}{\ln C/C_{eq}} - R\right) \tag{5}$$

$$R_0 = \frac{2\gamma v_{at}}{kT} \tag{6}$$

where the first term counts for growth of existing precipitates while the last term counts for the arrival of dN new nuclei.

For the growth and coarsening regime the model uses Eqs. (7) and (8).

$$\begin{cases} \left.\dfrac{dR}{dt}\right|_{growth} = \dfrac{D}{R}\dfrac{C - C_{eq}\exp(R_0/R)}{1 - C_{eq}\exp(R_0/R)} \\ \left.\dfrac{dN}{dt}\right|_{growth} = 0 \end{cases} \tag{7}$$

$$\begin{cases} \left.\dfrac{dR}{dt}\right|_{coars} = \dfrac{4}{27}\dfrac{C}{1 - C_{eq}}\dfrac{R_0 D}{R^2} \\ R = R^* = \dfrac{R_0}{\ln(C/C_{eq})} \end{cases} \tag{8}$$

Simple criteria considering the evolution of the precipitate density are used to determine the transitions between the different regimes [4].

5.2. Parameters of the model and their evolution with temperature

The present model includes a limited number of parameters, which all have a physical meaning.

- Equilibrium concentration, it was adjusted according to an exponential law, $C_{eq} = C^0_{eq}\exp(-Q_c/kT)$ in order to obtain $C_{eq} = 1\%$ at 160°C and $C_{eq} = 5.4\%$ at 400°C, which corresponded to DSC experiments. The initial solute concentration is taken as the sum of the atomic concentrations of Mg and Zn, namely 3.76%.
- Diffusion constant, it follows an Arrhenius law, and was adjusted in order to describe the kinetics at all temperatures. The resulting parameters are $D_0 = 6.4 \times 10^{-8}$ m^2 s^{-1} and $E_d = 1$ eV.
- Interfacial energy, it was also adjusted to the experimental results, but taken constant over the temperature range considered, at a value of 280 mJ m^{-2}.

The differences in behavior at different temperatures resulting from different nucleation mechanisms will thus appear in the temperature dependence of ΔG_0.

5.3. Results of the modeling

The best fits for the evolution of precipitate radius with time at the various temperatures between 120 and 170°C are shown in Fig. 7a–e. For each temperature, the evolution of the solute concentration predicted by the model is also represented in Fig. 8. As expected, the faster evolution of precipitate radius as the temperature increases is also associated with a faster decrease of the solute concentration. The model is able to predict correctly the precipitation kinetics at all temperatures within the stability range of η' with a single adjustable parameter ΔG_0. For the 120°C heat treatment, we can obtain a reasonable fit for aging times longer than 6 h. At shorter aging times at this temperature the precipitation is dominated by GP-zones rather than η', and thus, we cannot expect the model to give correct values without changing the parameters.

It is now interesting to discuss the values for the activation energies chosen at the different temperatures to obtain the best fit with the experimental data. First it is useful to recall the theoretical value for ΔG_0 if nucleation was homogeneous.

$$\Delta G_0 = \frac{16}{3}\pi\left(\frac{v_{at}}{kT}\right)^2\gamma^3 \tag{9}$$

Thus one can expect that at constant nucleation mechanism (in terms of heterogeneous nucleation, this would correspond to a constant wetting angle),

ΔG_0 should change with temperature proportionally to T^{-2}.

Fig. 9 shows that the evolution of $\Delta G_0 T^2$ with temperature is perfectly linear and not constant. A change in ΔG_0 could be connected to a change in the interfacial energy γ, but as we consider only one nature of precipitates, namely η', there is no reason why γ should change considerably. An increase in the interfacial energy of 30% over 50 K would be necessary to explain the increase in ΔG_0. The interesting outcome of this result is that it reflects different nucleation mechanisms acting over this temperature range. However, the detailed evolution of the nucleation barrier, namely $\Delta G_0 T^2 \propto T$, is probably a mere coincidence. The results are in agreement with the general accepted nucleation sequence in this system, it is known that nucleation of η' is very sensitive to the degree of clustering of the structure, in terms of VRC or GP zones [2,3,12]. In the thermal cycle that we have used in this study, the degree of clustering before the rapid heating to the aging temperature is very limited, and thus these clusters are likely to dissolve partially before any nucleation may occur. Therefore, it is expected that the higher the aging temperature, the more difficult the nucleation of η', due to larger dissolution of the potential nucleation sites in the ramping stages.

The fact that nucleation is difficult in these heat treatment conditions is confirmed by the comparison between the isothermal 150°C and the T6 aging procedures, the longer low temperature preheating in the case of T6 results in a higher density of η' nucleation sites, and thus in a lower precipitate radius in the first stages of aging.

Finally, it is interesting to compare the result of the model in terms of solute decay to the measured integrated intensity of SAXS spectra (which is an undirect measurement of the precipitated volume fraction). By using Eq. (2), we can compare the measured precipitated volume fraction to the volume fraction predicted by the model. As shown in Fig. 9 for the 140°C heat treatment, a good correspondence is obtained if we consider that the Zn/Mg ratio of the precipitates composition is 2.5, which is close to 2 for $MgZn_2$.

6. Conclusion

In the present paper, we have characterized the precipitation kinetics quantitatively over a range of temperatures. The simple model proposed in [4] modified for using a whole temperature range allows us to describe the kinetics for both precipitate radius and precipitated volume fraction with a limited number of adjustable parameters whose physical meaning and order of magnitude are known. The evolution of the only temperature dependent parameter ΔG_0, reflects the important changes in nucleation mechanisms which are encountered in the various heat treatment conditions, namely precipitation on GP zones or VRC's. The fact that the model is capable of describing such different nucleation conditions proves its versatility. In future work, it will have to be further adapted to describe more complex thermal histories, which may involve non-isothermal heat treatments.

Acknowledgements

The authors would like to thank Hydro Raufoss Automotive Technology Center for providing the materials and for financial support. We would also thank Dr Frederic Livet at LTPCM for helping with the experiments.

References

[1] G. Groma, E. Kovacs-Csetenyi, Phil. Mag. (1975) 869.
[2] T. Ungar, J. Lenvai, I. Kovacs, Aluminum 55 (1979) 663.
[3] H. Loffler, O. Kabisch, B. Gueffroy, M. Radomsky, G. Honyek, T. Ungar, Kristall Technik 14 (1979) 721.
[4] A. Deschamps, Y. Brechet, Acta Mater. 47 (1999) 293–305.
[5] O. Glatter, O. Kratky, Small Angle X-ray Scattering, Academic Press, New York, 1982.
[6] A. Deschamps, Y. Brechet, Mater. Sci. Eng. A251 (1998) 200–207.
[7] V. Hansen, L. Berg, J. Gjønnes, Internal report, University of Oslo, 2000.
[8] A. Deschamps, Y. Brechet, P. Guyot, F. Livet, Z. Metallkd. 88 (1997) 601–606.
[9] X.Z. Li, V. Hansen, J. Gjønnes, L.R. Wallenberg, Acta Mater. 44 (1999) 9.
[10] G. Waterloo, V. Hansen, J. Gjønnes, S.R. Skjervold, Mater. Sci. Eng. A, in press.
[11] H. Löffler, I. Kovacs, J. Lendvai, J. Mater. Sci. 18 (1983) 2215.
[12] T. Ungar, J. Lenvai, I. Kovacs, G. Groma, E. Kovacs-Csetenyi, Z. Metallkd. 67 (1976) 683.
[13] J. Lendvai, G. Honyek, I. Kovacs, Scr. Met. 13 (1979) 593.